Generation of Giga-electron-volt Proton Beams by Micronozzle Acceleration

M. Murakami

Institute of Laser Engineering, Osaka University

Our proposed ion acceleration scheme, micronozzle acceleration (MNA), generates proton beams with extremely high kinetic energies on the giga-electron-volt (GeV) order. The underlying physics and performance of MNA are studied with two-dimensional particle-in-cell simulations. In MNA targets, a micron-sized hydrogen rod is embedded inside a hollow micronozzle. Subsequent illumination of the target along the symmetric axis by an ultraintense ultrashort laser pulse forms a strong electrostatic field with a long lifetime and an extensive space around the downstream tail of the nozzle. The electric field significantly amplifies the kinetic energies of the accelerated protons, and ≳ GeV protons are generated at an applied laser intensity of 10^{22} W/cm².

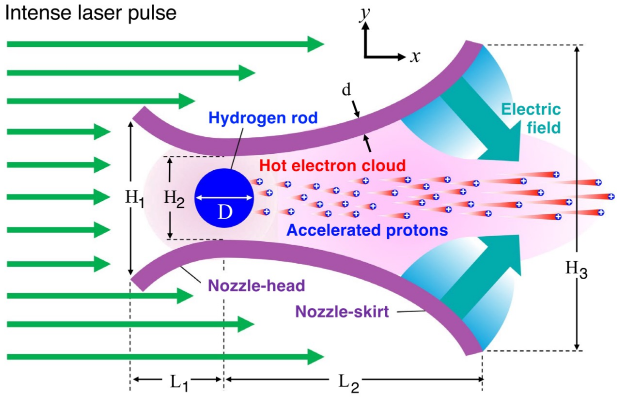

Fig. 1. A cross-sectional schematic view of MNA target. MNA target employs a micronozzle housing a solid hydrogen rod (H-rod), which is placed at around the nozzle-neck to maximize the proton emissio Aluminum is here employed as the nozzle material just as an example. The role of the micronozzle can understood as a kind of power lens, as it were, to integrate the applied laser energy onto the tiny H-rod about significantly higher energies than without the nozzle structure.

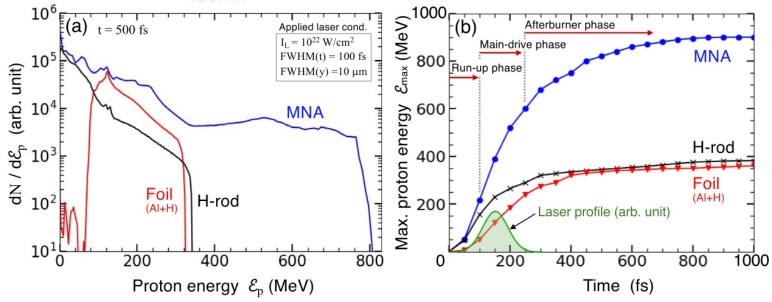

Fig. 4. **(a)** The proton energy spectra for the MNA, the H-rod, and the foil targets. The H-rod (2μm-diameter) is just the bullet body taken out from the MNA target, while the foil target is composed of a 1μm-thick aluminum with 50nm-thick solid hydrogen layer over-coated on the rear surface. **(b)** The temporal evolution of the three cases of **(a)**. For the MNA target, the maximum proton energy $\mathcal{E}_{\max}$ is read to be increasing at the rate of 160 MeV/100 fs even after the laser illumination is finished at $t \simeq 250$fs.

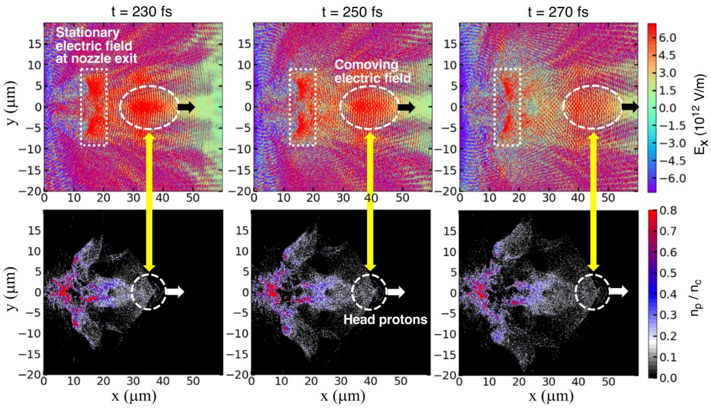

Fig. 5. Upper row: 2D profiles of the longitudinal electric fields E_x(compare Fig. 1). Lower row: proton density profiles at different times, at sequential times, $t = 230, 250$, and 270 fs for the MNA target, which correspond to the early times of the afterburner phase; n_c denotes the critical density. The head protons are observed to be continuously accelerated by the comoving electric field. Applied laser and target conditions are the same as in Fig. 3.

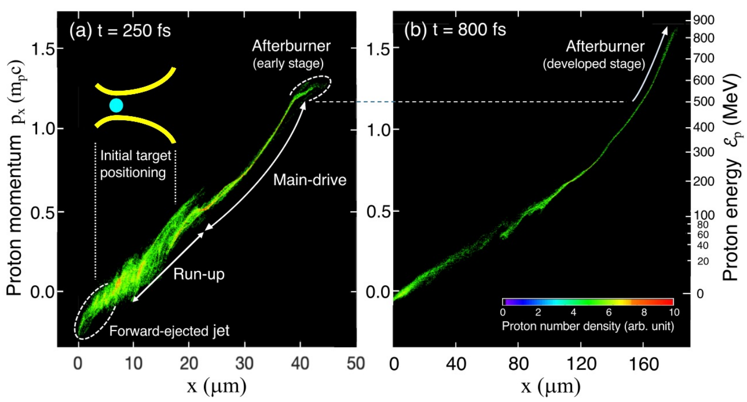

Fig. 6. The phase space plots at t = 250 fs and 800 fs, showing how the protons are accelerated through the three different phases. The proton energies increase mainly after they are ejected out of the nozzle through the main-drive and the afterburner phases.

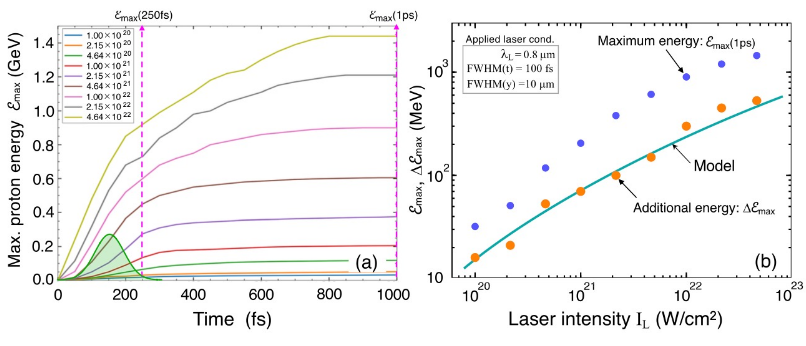

Fig. 7. **(a)** Temporal evolution of the maximum proton energies at different peak laser intensities (the upper-left inset in units of W/cm²). The green Gaussian profile denotes the laser pulse. The time, $t = 250$ fs, is taken here as the beginning of the afterburner phase. **(b)** Maximum proton energies at the end, $\mathcal{E}_{\max}$(1 ps) (blue circles), and the additional energies gained in the afterburner phase, $\Delta\mathcal{E}_{\max} = \mathcal{E}_{\max}$(1 ps) $-\mathcal{E}_{\max}$(250 fs) (orange circles). The solid curve is obtained by a simple analytical model based on a self-similar analysis.

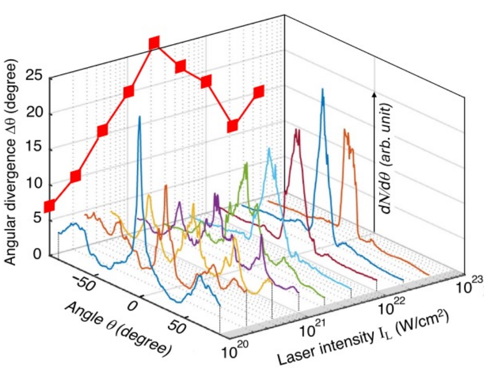

Fig. 10. Summary on the angular distributions of the proton beams, $dN/d\theta$, at different laser intensities, where the angle θ is measured with respect to the x-axis. The coherent results for the maximum proton energy $\mathcal{E}_p$ are given in Fig. 8 as the blue circles. The red squares on the vertical plane denote the angular divergences (FWHM), $\Delta\theta(I_L)$, obtained from the individual curves of $dN/d\theta$.